



1 A high-spatial resolution soil carbon and nitrogen dataset for the
2 northern permafrost region, based on circumpolar land cover
3 upscaling

4

5

6 Juri Palmtag¹, Jaroslav Obu², Peter Kuhry^{3, 4}, Andreas Richter⁵, Matthias B. Siewert⁶, Niels Weiss⁷;
7 Sebastian Westermann² and Gustaf Hugelius^{3,4}

8 ¹Department of Human Geography, Stockholm University, Stockholm, Sweden; ²University of Oslo,
9 Department of Geosciences, Sem Sælands vei 1, 0316 Oslo, Norway; ³Department of Physical Geography,
10 Stockholm University, Stockholm, Sweden; ⁴Bolin Centre for Climate Research, Stockholm University,
11 Stockholm, Sweden; ⁵ Centre for Microbiology and Environmental Systems Science, University of Vienna,
12 Vienna; ⁶Department of Ecology and Environmental Science, Umeå University, Umeå, 901 87, Sweden;
13 ⁷Northwest Territories Geological Survey, Government of the Northwest Territories, Yellowknife NT X1A
14 1K3, Canada.

15

16 Corresponding author: Juri Palmtag (juri.palmtag@humangeo.su.se)

17

18

19

20

21



22 Abstract

23 Soils in the northern high latitudes are a key component in the global carbon cycle; the northern permafrost region
24 covers 22% of the Northern Hemisphere and holds almost twice as much carbon as the atmosphere. Permafrost soil
25 organic matter stocks represent an enormous long-term carbon sink which is in risk of switching to a net source in the
26 future. Detailed knowledge about the quantity and the mechanisms controlling organic carbon storage is of utmost
27 importance for our understanding of potential impacts of and feedbacks on climate change. Here we present a
28 geospatial dataset of physical and chemical soil properties calculated from 651 soil pedons encompassing more than
29 6500 samples from 16 different study areas across the northern permafrost region. The aim of our dataset is to provide
30 a basis to describe spatial patterns in soil properties, including quantifying carbon and nitrogen stocks, turnover times,
31 and soil texture. There is a particular need for spatially distributed datasets of soil properties, including vertical and
32 horizontal distribution patterns, for modelling at local, regional or global scales. This paper presents this dataset,
33 describes in detail soil sampling, laboratory analysis and derived soil geochemical parameters, calculations and data
34 clustering. Moreover, we use this dataset to estimate soil organic carbon and total nitrogen storage estimates within
35 the soil area of the northern circumpolar permafrost region (17.9×10^6 km²) using the ESA's Climate Change Initiative
36 (CCI) Global Land Cover dataset at 300 m pixel resolution. We estimate organic carbon and total nitrogen stocks on
37 a circumpolar scale (excluding Tibet) for the 0-100 cm and 0-300 cm soil depth to 380 Pg and 813 Pg for carbon and
38 21 Pg and 55 Pg for nitrogen, respectively. Of which 48% of the area is within the land cover class forest with a total
39 SOC and TN storage for 0-300 cm of 35% and 36%, respectively. Our organic carbon estimates agree with previous
40 studies, with most recent estimates of 1000 Pg (– 170 to +186 Pg) to 300 cm depth but show different spatial patterns.
41 Two separate datasets are freely available on the Bolin Centre Database repository
42 (<https://doi.org/10.17043/palmtag-2022-pedon-1>, Palmtag et al., 2022a and [https://doi.org/10.17043/palmtag-](https://doi.org/10.17043/palmtag-2022-spatial-1)
43 [2022-spatial-1](https://doi.org/10.17043/palmtag-2022-spatial-1), Palmtag et al., 2002b).

44 1. Introduction

45 Permafrost soils represent a large part of the terrestrial carbon reservoir and form a significant and climate-sensitive
46 component of the global carbon cycle (Hugelius et al., 2014). High-latitude ecosystems are experiencing rapid climate
47 change causing warming of soil temperatures, thawing of permafrost, and fluvial and coastal erosion (Biskaborn et
48 al., 2019; Fritz et al., 2017). Warming enhances the decomposition of organic matter by microorganisms, which in
49 turn produces carbon dioxide, methane, and nitrous oxide. The release of these greenhouse gases to the atmosphere is
50 accelerating and could potentially constitute a positive feedback on global warming (Turetsky et al., 2020). To better
51 predict the magnitude and effect of environmental changes in the permafrost region, improved data on the properties
52 and quantities of carbon and nitrogen stored in these climate vulnerable soils are needed.

53 In many cases, a lack of observational data for parameterization or evaluation can limit model development or accurate
54 model projections (Flato, 2011). Soil properties such as organic matter (OM) content, soil texture and soil moisture or
55 their derivatives are commonly used to parametrize, train or validate models (e.g. Oleson et al., 2010). Yet, the

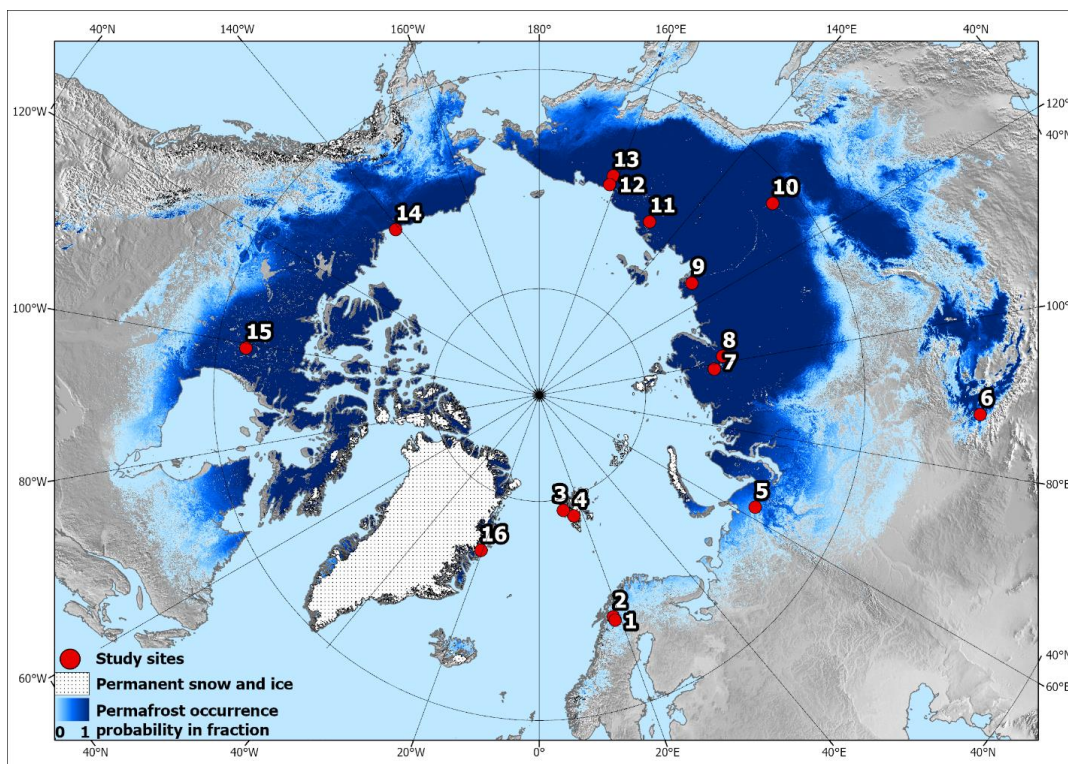


56 representation of northern soil profiles in global datasets remains limited (Köchy et al., 2015; Batjes, 2016), the
57 northern circumpolar permafrost region ($20.6 \times 10^6 \text{ km}^2$) in which permafrost can occur accounts for 22% of the
58 Northern Hemisphere exposed land area (Obu et al, 2019).

59 Many previous studies have shown a robust relationship between land cover and soil organic carbon (SOC)
60 distribution, making land cover datasets useful for upscaling from soil profiles to full landscape coverage (e.g. Kuhry
61 et al., 2002; Hugelius, 2012; Palmtag et al., 2015; Siewert et al., 2015; Wojcik et al., 2019). Here we describe the
62 compilation of a harmonized soil dataset for permafrost-affected landscapes derived from 15 different high latitude
63 sites and one high alpine study site in Canada, Greenland, Svalbard, Sweden, and Russia (Fig. 1; Table 1). In total,
64 651 soil pedons contain information from up to 6529 samples on carbon and nitrogen content, carbon to nitrogen
65 (C/N) ratio, isotopic composition, texture (sand, silt+clay) and coarse fraction content, land cover type, wet and dry
66 bulk density, calculated volumetric contents for ice/water, and volumetric content of organic soil material, mineral
67 soil material and air. In addition, soil pedon descriptions include metadata on actual sampling site, coordinates and
68 elevation, slope and aspect, drainage, cover stones and boulders, landform, and maximum sampling depth. Site data
69 was upscaled to the northern circumpolar permafrost region using the European Space Agency (ESA) Climate Change
70 Initiative (CCI) Global Land Cover dataset at 300 m pixel resolution, which is the very first long-term global land
71 cover time series product.

72 This study has two main objectives. Firstly, the core objective of this dataset is to provide a harmonized, high
73 resolution, quality controlled, and contextualized soil pedon dataset with a focus on SOC, nitrogen and other
74 parameters essential to determine the role of northern permafrost region soils in the climate system. Secondly, to use
75 the dataset and an existing spatial product for upscaling to provide a new and independent estimate of the soil organic
76 carbon and total nitrogen (TN) storage estimates within the northern circumpolar permafrost region. The data set aims
77 to provide the scientific community with new and improved geospatial products quantifying carbon and nitrogen pools
78 within the northern circumpolar permafrost region. Particularly, the extensive metadata on soil properties included for
79 many samples when available (texture, volumetric densities, active layer depth, ice content, isotopic composition, etc.)
80 are of great importance and can be used to identify and model the processes responsible for the current and future
81 carbon balance.

82



83

84 Figure 1: Overview map with location of the 16 sampling sites (see Table 1). Blue shading indicates permafrost
85 probability (dark hues showing higher permafrost occurrence probability), based on an equilibrium state model for
86 the temperature at the top of the permafrost (TTOP) for the 2000–2016 period (Obu et al., 2019). North Pole Lambert
87 azimuthal equal area projection (datum: WGS 84). Base map: Made with Natural Earth.

88

89

90 2. Dataset structure

91 The dataset contains 6529 analyzed samples from 651 soil pedons in 16 different sampling locations across the
92 northern permafrost region (Fig 1; Table 1) (Palmtag et al., 2022a, b). Each sampled pedon was described and
93 classified according to land cover type. Land cover is defined as the biophysical cover of the Earth's terrestrial surface
94 such as different vegetation types, water, and bare ground.

95



96 Table 1: Summary of all study sites

Nr.	Study area	Country	Long	Lat	n=pedons	Reference
1	Tarfala	Sweden	18.63	67.91	55	Fuchs et al., 2015
2	Abisko	Sweden	18.05	68.33	125	Siewert, 2018
3	Ny Ålesund	Norway	11.83	78.93	28	Wojcik et al., 2019
4	Adventdalen	Norway	16.04	78.17	48	Weiss et al., 2017
5	Seida, Usa River Basin	Russia	62.55	67.35	44	Hugelius et al., 2009; 2011
6	Aktru, Altai mountains	Russia	87.47	50.05	39	Pascual et al., 2020
7	Logata, Taymyr	Russia	98.42	73.43	31	Palmtag et al., 2016
8	Arymas, Taymyr	Russia	101.90	72.47	35	Palmtag et al., 2016
9	Lena Delta	Russia	126.22	72.28	56	Siewert et al., 2016
10	Spasskaya Pad	Russia	129.46	62.25	33	Siewert et al., 2015
11	Tjokurdach	Russia	147.48	70.83	27	Siewert et al., 2015; Weiss et al., 2016
12	Shalaurovo	Russia	161.55	69.32	22	Palmtag et al., 2015
13	Cherskiy	Russia	161.30	68.45	15	Palmtag et al., 2015
14	Herschel Island	Canada	-139.09	69.58	42	Siewert et al., 2021
15	Tulemalu Lake	Canada	-99.16	62.55	16	Hugelius et al., 2010
16	Zackenbergl	Greenland	-20.50	74.45	35	Palmtag et al., 2015; 2018

97

98

99 Land cover products are commonly satellite derived and sometimes globally available. We opted for a two-tier
100 approach, where more classes can be used in products with higher thematic or spatial resolution (Table 2). First, we
101 differentiated land cover into 7 primary tier classes (Tier I) which represent the major land cover types: Forest, Tundra,
102 Wetland, Water, Barren, Permanent Snow/Ice and Yedoma. Although Yedoma is a sedimentary deposit and not a
103 typical land cover class, it was added due to its large areal extent, special soil organic matter (SOM) and ground ice
104 properties, as well as soil characteristics (Strauss et al., 2017; Weiss et al., 2016). Subsequently, Tier I classes were
105 subdivided into 14 Tier II subclasses (Table 2). The two-class tier structure provides more detailed information for
106 each specific land cover class. Depending on the accuracy of the land cover data available for specific sampling sites,
107 the best fitting Tier level can be used.

108



109

110 Table 2: Hierarchical structure of the two-tier land cover class system applied to the pedons based on field
111 observations.

TIER I		TIER II	
1	Forest	1.1	Deciduous broadleaf forest
		1.2	Evergreen needleleaf forest
		1.3	Deciduous needleleaf forest
2	Tundra	2.1	Shrub tundra
		2.2	Graminoid / forb tundra
3	Wetland	3.1	Permafrost wetlands
		3.2	Non-permafrost wetlands
4	Water bodies	4.1	Lakes
		4.2	Streams
5	Barren	5.1	Barren
6	Snow / Ice	6.1	Snow / Ice
7	Yedoma	7.1	Yedoma tundra
		7.2	Yedoma forest

112 2.1 Class definitions of soil pedons to land cover types

113 All pedons were assigned to land cover classes based on field observations and photographs. The forest class was used
114 for sparse to dense forests, further separated into three different Tier II classes: deciduous broadleaf, evergreen
115 needleleaf and deciduous needleleaf forest. Tundra is separated in Tier II to shrub tundra (dominated by erect shrubs
116 >50cm height) and graminoid / forb tundra (with low growth heath vegetation or graminoid dominated). Wetland
117 includes terrain that is saturated with water for sufficient time of the year to promote aquatic soil processes with low
118 oxygen conditions and occurrence of vegetation fully adapted to these conditions, as well as all types of peatlands.
119 The following types of wetlands described in the field were included to the wetland class: organic wetland, mineral,
120 seasonal, permanent, ombrogenous and minerogenous mires. Tier II wetland classes are wetlands with permafrost
121 within the upper 2 m from the soil surface and wetlands without permafrost within the upper 2 m from the soil surface.
122 Although a substantial part of the northern circumpolar permafrost region is classified as water ($0.98 \times 10^6 \text{ km}^2$) or
123 permanent snow/ice ($0.06 \times 10^6 \text{ km}^2$), no soil sample or pedon data from these classes are included in the database.
124 For the same reason the Tibetan permafrost region was not included in our estimates. The class barren includes land
125 cover types such as exposed bedrock, boulder fields, talus slopes, debris cones, rock glaciers, where soil is either



126 completely absent, or occurs only in minor patches (<10% area) or in between boulders. The land cover class Yedoma
127 is defined as areas underlain by late Pleistocene ice-rich syngenetic permafrost deposits, which occupy an area of
128 about 1,000,000 km² in Siberia, Alaska, and Yukon (Strauss et al., 2017). Tier II divides the Yedoma domain into
129 Yedoma tundra and Yedoma forest.

130 **2.2 Soil sampling and soil analyses**

131 The main aim of the field studies compiled in the current dataset was to perform SOC/TN pool inventories of each
132 study area considering different land cover types, geomorphological landforms and soil properties. Field soil sampling
133 took place in summer months (late June to early September) between 2006 and 2019, most frequently in August or
134 September in order to capture the maximum seasonal thaw (active layer) depth at each site. At most sites, a stratified
135 sampling scheme consisting of linear transects with predefined equidistant intervals of typically 100 to 200 m across
136 all major landscape elements was used. To ensure that this sampling scheme covered all representative landscape units
137 and types, maps (including vegetation, surficial geology) and remote sensing products (including air photos, satellite
138 imagery, and elevation models) were assessed prior to fieldwork. Detailed field reconnaissance involving visual
139 observation of the manageable study area were conducted before establishing transects. Sampling sites were located
140 and marked at the exact position based on distance to the first sampling point and compass bearing using a hand-held
141 GPS device. This ensured an unbiased location of individual sampling sites. For some locations, when sufficient time
142 was available in the field, a random or stratified random distribution of sampling points was used. Following the field
143 sampling protocol (Figure S1), a site description, soil and in several cases phytomass sampling were conducted at each
144 sampling point.

145 For each pedon, the top organic layer was sampled in three replicates, the active layer was sampled from an open soil
146 pit and deeper sections normally using a steel pipe for soil coring in permafrost. When possible, samples were also
147 collected from exposures along lake shores or river valleys (Fig. 2). Accurate determination of soil bulk density (BD)
148 is crucial when converting sample weight to volume or area and is essential to calculate SOC stocks. Therefore, special
149 attention was paid to accurate soil volume estimation during field sampling. The target depth for soil cores was 100
150 cm, or until bedrock or massive ground ice (e.g. ice-wedges) was reached. Pedons were occasionally extended beyond
151 100 cm depth, in particular to assess full peat depth and organic/mineral transition in organic soils.

152 The top organic layer samples were cut out as a block using a pair of scissors or a knife (removing living vegetation),
153 measuring the block volume in the field (Fig. 2). Variation in the top organic layer thickness can be substantial and
154 for this reason from most pedons two randomly selected replicates (OL2 & OL3) in addition to the main soil pit were
155 collected (not in peatlands). Active layer samples were collected from a soil pit excavated to the bottom of the active
156 layer, to the bedrock or to reach a depth of ± 50 cm, or in a few cases from natural exposures using 100 cm³ soil
157 sampling rings inserted horizontally into the soil profile. Sampling of the active layer was performed in fixed depth
158 intervals or along soil horizon boundaries. During some field campaigns, emphasis was also given to the spatial
159 distribution of soil horizons in the soil pit using perspective corrected photographs to calculate the respective area



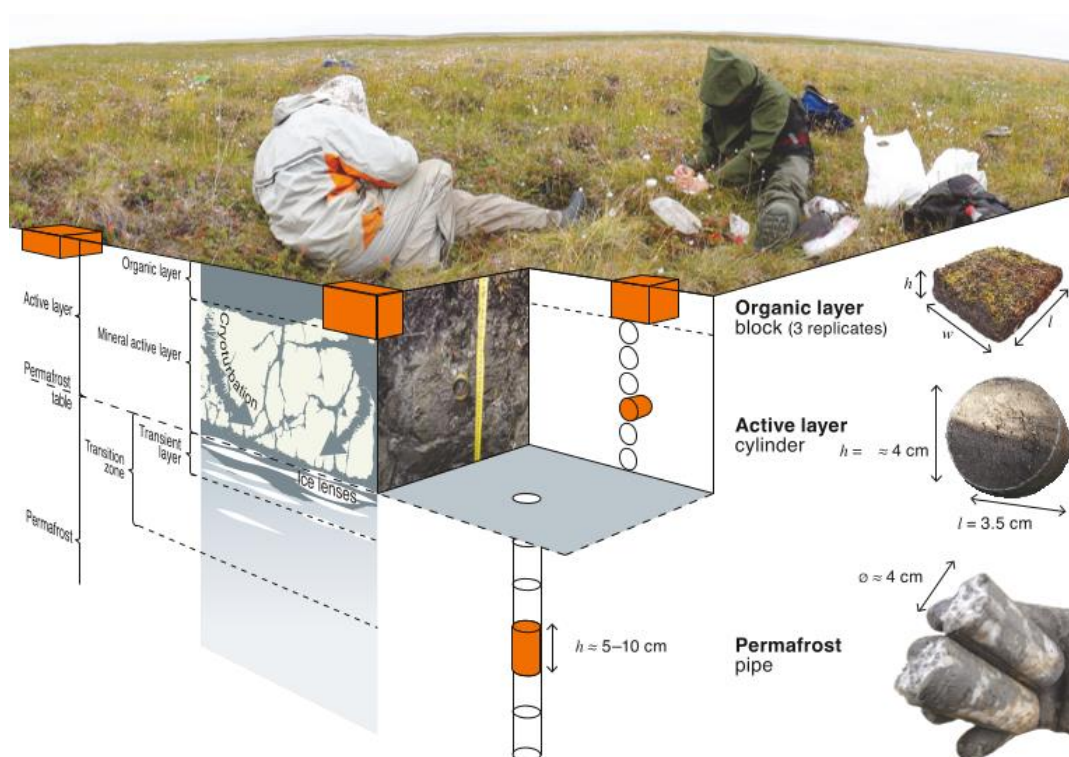
160 covered by each horizon, which was then translated into depth increments (Siewert et al, 2016; 2021). For permafrost-
161 free wetland sites a Russian peat corer with a 50 cm long chamber was used. After extraction, the core was described
162 and subdivided into smaller increments (generally 5 cm). This resulted typically in about 5–15 samples per sampling
163 site depending on the reached depth.

164 The permafrost section of the soil profile and very deep unfrozen soil layers were sampled using a steel pipe that was
165 hammered into the frozen ground in short (5 to 10 cm) depth increments. The pipe was pulled out after each sampled
166 increment using large pipe wrenches, and the sample was pushed out of the pipe using a steel rod. These steel pipes
167 are industry standardized with an outer diameter of 42.2 mm (1.25 inches), affordable and widely available even in
168 remote locations. A custom-made protective hard-steel cap placed over the steel pipe greatly extends the usability of
169 the pipe and this method in general. Over time, pipe-ends deform from hammer impacts and hard objects such as
170 rocks, and damaged ends can be cut off in the field using a hacksaw. An experienced team of 2-3 persons can sample
171 4-6 soil pedons in one day using this method. At several locations, soil cores were collected using a handheld
172 motorized rotational Earth Auger (Stihl BT 121) with a 50 cm core barrel and 52 mm outside diameter. Following
173 recovery, samples were split lengthwise in preparation for analysis. Usually, half of each core was kept as a frozen
174 archive to be used in the event of laboratory error. The remaining half-core was analyzed to determine sediment
175 characteristics, volumetric ice content, and gravimetric water content. Disturbance material was removed from the
176 core surface by repeated scraping with a razor blade. All half-cores were then photographed and described in detail.

177 All samples were described in the field and packed into sampling bags. Wet or frozen samples were placed in double
178 bags to assure no soil water was lost in transport. For each sampled soil profile, pictures and notes were taken to
179 describe land cover type, landform, elevation, slope and aspect, surface moisture, and surface features. Specific
180 observations regarding the collected sample depths, such as excess ground ice (visual estimate, %), occurrence of
181 large stones (visual estimate, %), colour (general description or using a Munsell scale), soil structure, including signs
182 of cryoturbation, roots and rooting depth were noted. Samples with cryoturbated soil material were marked or rated
183 on a scale from 1 to 3 according to the relative amount of cryoturbated soil material. Soil texture, which refers to
184 particle size and relative content of mineral components (sand, silt+clay) is of importance as it affects the physical
185 and chemical properties of a soil, including cryoturbation (Palmtag and Kuhry, 2018). Soil texture was estimated for
186 most samples using manipulation tests and assessment by hand in the field under varying weather conditions.
187 Therefore, we decided to combine silt and clay to avoid misinterpretation and refer to them as one fine-grained soil
188 texture class. For a subset of samples, particle size analysis was performed using a Malvern Mastersizer 3000 laser
189 particle size analyzer (Malvern Instruments Ltd, Malvern, UK), which can analyze particles in the range of 0.01–3500
190 μm in diameter. It measures the intensity of light scattered as a laser beam passes through a dispersed particulate
191 sample. A detailed description of these samples is given in Palmtag et al. (2018). For some studies soils were classified
192 following the US Soil Taxonomy system (Soil Survey Staff, 2014). The availability of these parameters is consistent
193 for most pedons, but the degree of metadata completeness depends on the scope of the original study. The land cover
194 and vegetation community was described at all sites. For many sites, vegetation cover was described in terms of



195 relative plant functional type coverage per square meter. Beyond assigning the profiles to land cover, vegetation data
196 is not included in this database and not further discussed.



197

198 Figure 2: A three-dimensional field sampling protocol with typical soil layers in permafrost ground (reprinted from
199 Weiss 2017, p.12). The orange shapes represent the different sampling techniques for organic surface layer (block),
200 active layer sample from an excavated pit (fixed volume cylinder) and permafrost sampling (steel pipe).

201 2.3 Laboratory analysis

202 In the laboratory, soil samples (n=6529) were weighed before and after oven-drying at 60-70°C for at least 24h (or
203 until no further weight change was observed) to determine field-moist mass (m_{ws}), oven-dried mass (m_d), wet bulk
204 density (BD_w) and dry bulk density (BD , $g\ cm^{-3}$). In most cases, subsamples of around 10g were dried again at 105°C
205 to verify dry weight and correct in case not all water was lost at the lower temperature. The reason for the main sample
206 being dried at lower temperature is to ensure that samples can be dried in the original plastic sample bags (without
207 loss of sampled materials) and subsequently used for additional analyses that may be sensitive to the higher drying
208 temperature (results from such additional analyses are not included here). After drying, samples were homogenized
209 and sieved to determine the concentration of coarse mineral fragments (CF, >2 mm, %). Subsamples (n=4488) were
210 burned for 5h at 550°C to obtain organic matter content through loss on ignition (LOI; Heiri et al., 2001), and about



211 every second sample (n=2976), was burned at 950°C for 2h to determine carbonate content (for details, see Palmtag
212 et al., 2015; 2016). To determine the elemental content of carbon and nitrogen (TOC and TN) and their isotopic
213 composition, 2496 samples were analysed using an Elemental Analyser (EA). If LOI indicated presence of inorganic
214 carbon, samples were acid treated with hydrochloric acid prior to determination of TOC. To estimate the organic
215 carbon % for samples where only LOI was available, a regression was performed between LOI550 and %C from EA
216 on samples for which both analyses were available. In most cases a third or fourth order polynomial regression model
217 was used and applied at study area level.

218 Carbon to nitrogen (weight) ratios are often used as an indicator for SOM decomposition. As during the metabolic
219 activity by microorganisms more carbon than nitrogen is released, the C/N ratio decreases with a higher degree of
220 humification. This is why C/N ratios usually decrease with depth, as deeper layers are typically older and underwent
221 decomposition over longer periods of time (Kuhry and Vitt, 1996). Together with stable carbon isotopes ($\delta^{13}C$) this
222 can be used to gain insight into the biochemical processes of SOM, botanical origin with depth and the degradation
223 state (Kracht and Gleixner, 2000).

224 **2.4 Calculations and soil profile extrapolations**

225 Dry and wet bulk density ($g\ cm^{-3}$), sample volume (cm^3) and % carbon was used to calculate the volumetric contents
226 of water, organic soil material, mineral soil material and air for each sample. The soil organic carbon content (kgC
227 m^{-2}) was calculated for each sample separately based on dry bulk density (BD, $g\ cm^{-3}$), percentage organic C in the
228 sample (%C), sample thickness T (cm), and coarse fraction correction (CF) (Equation 1). Equation 1 was also used to
229 calculate the TN content, in which %C was replaced with %N.

$$230\quad SOC(gCm^{-2}) = BD * \%C * (1 - CF) * T \quad 1$$

231 SOC content for each pedon was calculated by summing up individual samples to a specific depth (30 cm, 50 cm, 100
232 cm, 100-200 cm, 200-300 cm, and 0-300 cm) until the maximum sampling depth was reached. In areas with large
233 stones in the soil column (e.g. alpine areas) or areas with massive ice bodies (e.g. Yedoma deposits), it is also important
234 to deduct the volume of stones or massive ice from the calculations. These additional variables are not included in
235 equation 1, but were accounted for in the SOC calculations at the pedon level. If bedrock was encountered at any
236 point, a SOC content of $0\ kg\ C\ m^{-2}$ was assigned for the remaining part down to 300 cm depth at that specific sampling
237 site. For calculations, the top organic layer calculation is based on the first OL1 sample only. In pedons where some
238 increments were missing or the full sampling depth was not reached, the nearest samples from the same pedon for BD
239 and %C were interpolated or extrapolated. To avoid overestimation of the SOC storage, such extrapolations were only
240 used where field notes showed that the deposits were homogeneous and bedrock was not reached.

241 Masses of soil components (water (m_w , g), organic matter (m_{OM} , g) and mineral component (m_{min} , g)) were calculated
242 from laboratory results. The mass of water was calculated as a difference between field-moist mass and oven-dried
243 mass. Organic matter mass was calculated from the %C and dry sample weight and multiplied by 2, which is a standard



244 conversion factor between SOC and SOM (Pribyl, 2010). The mass of the mineral fraction was calculated as a
245 difference between dry sample mass and organic matter mass.

246 Volumetric fractions of soil components were calculated by dividing the volume of the component with the total
247 sample volume (V). We calculated component volumes from mass by assuming the following densities: 1 g/cm³ for
248 water, 0.91 g/cm³ for ice, 1.3 g/cm³ for organic matter (Farouki, 1981) and 2.65 g/cm³ mineral component. The
249 volumetric fraction of air was calculated as one minus the sum of the other fractions.

250 **2.5 Pedon grouping and SOC/TN upscaling**

251 All profiles were assigned to land cover class based on field descriptions. Dry bulk density, SOC density, TN density
252 and the volumetric contents of mineral and organic matter and water and air were averaged according to land cover
253 classes for depths until 3 m using Python scripting language and pandas library (McKinney, 2011). Soil parameters
254 were assigned to pedon sample depth ranges and these were grouped according to land cover classes yielding means
255 and standard deviations for each centimetre of depth. Fractions of soil texture classes (sand and silt+clay) were created
256 using the same procedure by counting occurrences of texture classes within pedons. The values were averaged with 1
257 cm resolution for the top 10 cm, to 5 cm between 10 and 30 cm and to 10 cm averaged values for below 30 cm of soil
258 depth. Typical soil stratigraphies were generated for each class which can be used as input for permafrost modelling
259 and mapping (e.g. Westermann et al., 2013; 2017; Czekirda et al., 2019).

260 For the upscaling, we used the land cover map from the Global ESA Land cover Climate Change Initiative (CCI)
261 project at 300 m spatial resolution (<http://maps.elie.ucl.ac.be/CCI/viewer/index.php>). The overall classification
262 accuracy, based on 3167 random sampling cases, is stated as 73% (Defourny et al., 2008). The land cover class dataset
263 for upscaling was generated from ESA CCI land cover yearly products from period 2006 to 2015 (corresponding to
264 the sampling period) using majority statistics to define prevailing land cover classes within this period. The extent of
265 the Yedoma land cover classes was defined from shapefiles of the Yedoma database by Strauss et al., (2016), where
266 all the layers were used except for QG2500k, which is showing the lowest probability of Yedoma occurrence. While
267 the extent of Yedoma is based on maps of Quaternary deposits, no such maps were used to support upscaling of other
268 soil properties.

269 The spatial land cover extent was constrained to the Northern Hemisphere permafrost region indicating probability of
270 permafrost occurrence but not the actual area underlain by permafrost (indicated by permafrost area) (Obu, 2021). The
271 used permafrost region dataset stretches over 17.9×10^6 km² of the Northern Hemisphere, and is based on equilibrium
272 state model for the temperature at the top of the permafrost (TTOP) for the 2000–2016 period (Obu et al., 2019).

273 Since the ESA land cover product uses a different nomenclature for land cover types with different sub-categories,
274 similar classes were amalgamated to fit our tiered land cover system (Table 2). Several minor classes consisting of
275 single pixels spread over the map were generalized and merged with the class surrounding the pixel. The Tier classes
276 “water bodies” and “Snow / Ice” occupy substantial areas but were excluded from the SOC storage estimates; this



277 study focuses on terrestrial SOC and TN storage. We defined tier II Yedoma classes (Yedoma tundra and Yedoma
 278 forest) according to the ESA CCI Land cover classes coinciding with Yedoma deposits (Table 3).

279

280 Table 3: Amalgamation of ESA's CCI land cover classes with the Tier class system above the Yedoma deposits.

CCI class	ESA CCI landcover	TIER I class	TIER II class
40	Mosaic natural vegetation (tree, shrub, herbaceous cover) (>50%)	1	1.1 & 7.2
50	Tree cover, broadleaved, evergreen, closed to open (>15%)	1	1.1 & 7.2
60	Tree cover, broadleaved, deciduous, closed to open (>15%)	1	1.1 & 7.2
61	Tree cover, broadleaved, deciduous, closed (>40%)	1	1.1 & 7.2
70	Tree cover, needleleaved, evergreen, closed to open (>15%)	1	1.2 & 7.2
71	Tree cover, needleleaved, evergreen, closed (>40%)	1	1.2 & 7.2
72	Tree cover, needleleaved, evergreen, open (15-40%)	1	1.2 & 7.2
80	Tree cover, needleleaved, deciduous, closed to open (>15%)	1	1.3 & 7.2
90	Tree cover, mixed leaf type (broadleaved and needleleaved)	1	1.1 & 7.2
100	Mosaic tree and shrub (>50%) / herbaceous cover (<50%)	1	1.1 & 7.2
110	Mosaic herbaceous cover (>50%) / tree and shrub (<50%)	1	1.3 & 7.2
120	Shrubland	2	2.1 & 7.1
121	Evergreen shrubland	2	2.1 & 7.1
122	Deciduous shrubland	2	2.1 & 7.1
130	Grassland	2	2.2 & 7.1
140	Lichens and mosses	2	2.2 & 7.1
150	Sparse vegetation (tree, shrub, herbaceous cover) (<15%)	2	2.1 & 7.1
152	Sparse shrub (<15%)	2	2.1 & 7.1
160	Tree cover, flooded, fresh or brackish water	3	3.1
180	Shrub or herbaceous cover, flooded, fresh/saline/brackish water	3	3.1
200	Bare areas	5	5.1
201	Consolidated bare areas	5	5.1
202	Unconsolidated bare areas	5	5.1
210	Water bodies	4	4.1
220	Permanent snow and ice	6	6.1

281

282 The upscaling to estimate the total carbon storage in the northern circumpolar permafrost region was performed in
 283 ArcGIS Pro (ESRI, Redlands, CA, USA) by multiplying the mean SOC storage for each tier and tier 2 class with the
 284 spatial extent of the corresponding CCI land cover class. To determine reasonable error estimates for carbon stocks
 285 within the permafrost region, we used a spatially weighed 95% confidence interval (CI) as described by Thompson
 286 (1992) assuming that our residuals are normally distributed (Hugelius, 2012). The CI accounts for the relative spatial
 287 extent, carbon stock variations in pedons and number of replicates in each upscaling class. Replicates were only
 288 considered for pedons reaching the full depth, resulting in fewer replicates with increasing sampling depth. In equation



289 2: t is the upper $\alpha/2$ of a normal distribution ($t \approx 1.96$), α the % of the area; SD is the standard deviation, n is to the
 290 number of replicates and i refers the specific Tier class.

$$291 \quad CI = t * \sqrt{\sum((a_i^2 * SD_i^2)/n_i)} \quad 2$$

292 3. Results

293 3.1 SOC estimates

294 Using our pedon based dataset, we obtain SOC stock estimates within the northern circumpolar permafrost region of
 295 379.7 and 812.6 Pg for 0-100 cm and 0-300 cm depth, respectively. Table 4 shows mean SOC storage (kg C/m²) and
 296 total SOC stock for all depth increments, including 95% confidence intervals. The upscaling using this new pedon
 297 data shows that almost half of SOC in the northern circumpolar permafrost region is stored in the top meter. The three
 298 most abundant classes together (deciduous needleleaf forest, shrub tundra and graminoid / forb tundra) occupy 67%
 299 of the permafrost region (Table 5) and store the bulk of terrestrial SOC in the northern circumpolar region (74%). The
 300 permafrost wetland class has the largest SOC content to 300 cm with 112.2 kg C /m², but has only a small areal
 301 coverage in the ESA LCC product (1.4%) which results in a total SOC storage contribution of 3.5% within the
 302 permafrost region. Figure 3 illustrates the spatial distribution of total SOC storage (kg C m⁻²) to a depth of 300 cm for
 303 the circumpolar permafrost region.

304 Table 4: Landscape mean and total SOC storage with 95% CI for the different depth increments for the northern
 305 circumpolar permafrost region, excluding water bodies and permanent snow and ice.

Depth increment	n:	Landscape mean SOC storage (kg C/m ²)	95% CI ^a	Total SOC in Pg	95% CI ^a
0-30	452	9.0	± 1.4	160.0	± 25
0-50	402	12.8	± 1.8	229.3	± 32
0-100	328	21.3	± 3.2	379.7	± 58
100-200	257	12.4	± 1.9	222.0	± 35
200-300	253	11.8	± 1.7	211.0	± 31
0-300	253	45.5	± 7.6	812.6	± 136

306

307 ^a The 95% confidence interval refers to landscape mean SOC storage and total SOC storage



308 Table 5: Mean and total SOC storage for (A) 0-100 cm and (B) 0-300 cm soil depth separated for the different Tier
 309 classes in the northern circumpolar permafrost region, excluding water bodies and permanent snow and ice.

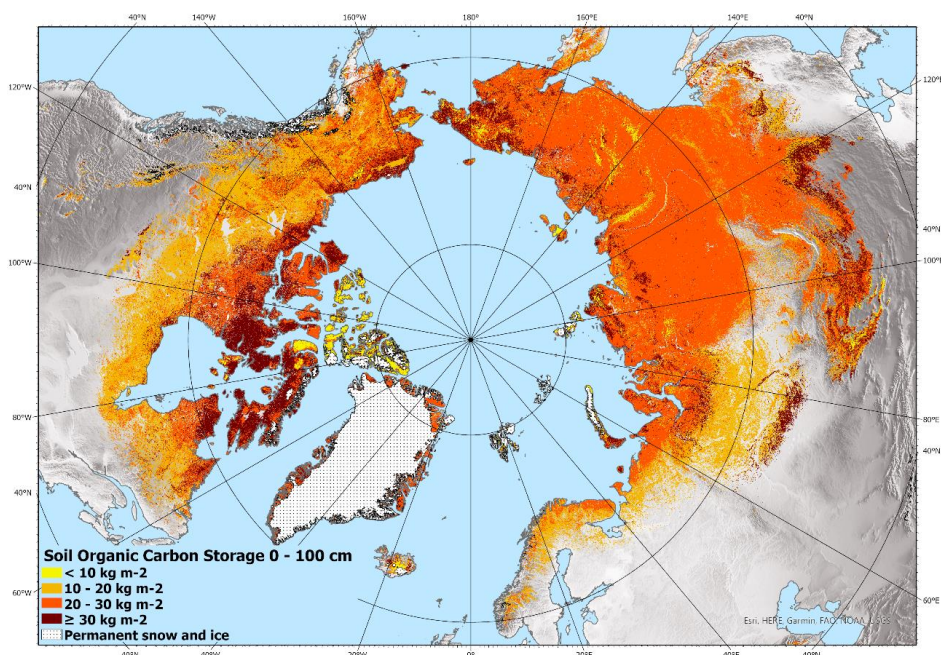
A	Tier class	LCC class	n ^a:	Area (million km²)	Area %	Mean SOC storage (kg C/m²) ^b	SD ^b	Total SOC in Pg	Total SOC storage %
1.1	Deciduous forest	broadleaf	5	0.85	4.8%	16.5	9.3	14.1	3.7
1.2	Evergreen forest	needleleaf	4	2.54	14.3%	14.6	12.8	37.1	9.8
1.3	Deciduous forest	needleleaf	28	5.20	29.1%	20.5	20.3	106.5	28.1
2.1	Shrub tundra		54	3.97	22.3%	22.3	21.7	88.5	23.3
2.2	Graminoid / forb tundra		118	2.85	15.9%	31.6	23.0	90.0	23.7
3.1	Permafrost wetlands		61	0.25	1.4%	37.8	37.8	9.6	2.5
3.2	Non-permafrost wetlands		10	0.76	4.3%	17.8	14.7	13.5	3.6
5.1	Barren		39	0.85	4.8%	9.4	12.0	8.0	2.1
7.1	Yedoma tundra		8	0.27	1.5%	28.1	17.0	7.7	2.0
7.2	Yedoma forest		1	0.30	1.7%	16.1	0.0	4.8	1.3

B	Tier class	LCC class	n ^a:	Area (million km²)	Area %	Mean SOC storage (kg C/m²) ^b	SD ^b	Total SOC in Pg	Total SOC storage %
1.1	Deciduous forest	broadleaf	2	0.85	4.8%	33.2	22.8	28.3	3.5
1.2	Evergreen forest	needleleaf	2	2.54	14.3%	23.0	16.3	58.7	7.2
1.3	Deciduous forest	needleleaf	14	5.20	29.1%	38.3	33.3	199.2	24.5
2.1	Shrub tundra		50	3.97	22.3%	49.2	50.8	195.6	24.1
2.2	Graminoid / forb tundra		114	2.85	15.9%	72.2	67.5	205.4	25.3
3.1	Permafrost wetlands		49	0.25	1.4%	112.2	121.5	28.4	3.5
3.2	Non-permafrost wetlands		7	0.76	4.3%	74.5	70.5	56.6	7.0
5.1	Barren		9	0.85	4.8%	11.7	14.9	10.0	1.2
7.1	Yedoma tundra		5	0.27	1.5%	64.1	37.7	17.5	2.2
7.2	Yedoma forest		1	0.30	1.7%	43.0	0.0	13.0	1.6

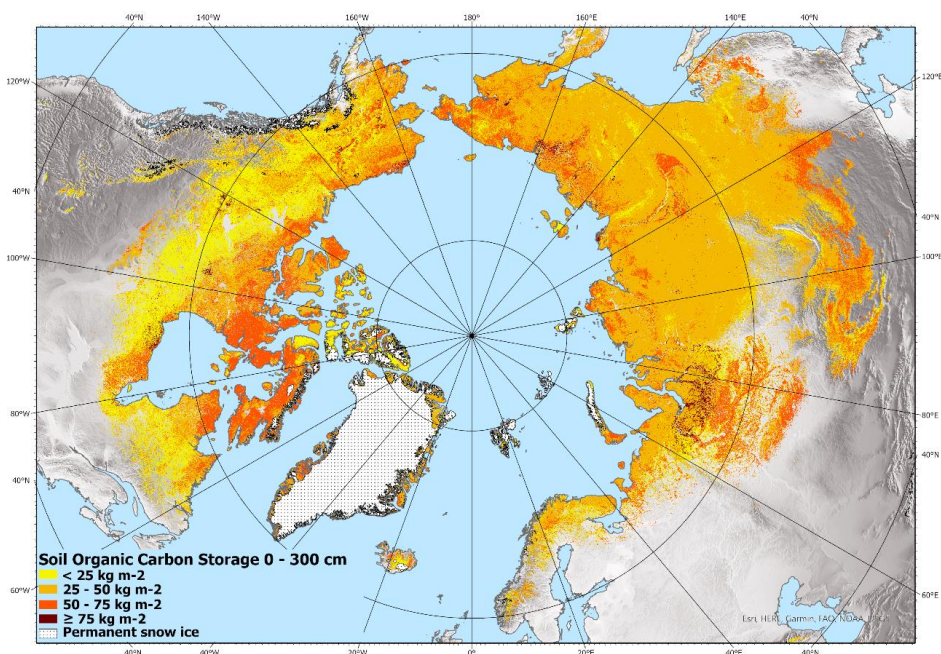
310

311 ^a The number of sampled pedons reaching a full depth of 100 cm or 300 cm, respectively.

312 ^b Mean SOC storage and SD calculations includes pedons which are not reaching the full section depth.



313



314

315 Figure 3. Estimated total SOC storage (kg C m^{-2}) to a depth of 0-100 cm and 0-300 cm in northern circumpolar
316 permafrost region. North Pole Lambert azimuthal equal area projection (datum: WGS 84). Base map: Made with
317 Natural Earth.



318 3.2 TN estimates

319 Our estimates show that the TN stocks down to 100 cm and 300 cm depth in the northern circumpolar permafrost
320 region are 21.1 Pg and 55.0 Pg, respectively. Table 6 presents the mean and total TN storage for different depth
321 increments with their 95% confidence interval. The TN distribution throughout the full depth is more evenly
322 distributed compared to SOC. As with SOC storage, the most abundant land cover classes (deciduous needleleaf forest,
323 shrub tundra and graminoid / forb tundra) store the bulk (68%) of the total TN in the permafrost region. The land
324 cover classes permafrost and non-permafrost wetlands have the largest TN storage with a mean of up to 7 kg /N m²
325 for the 0-300 cm soil depth (Table 7). Figure 4 illustrates the spatial distribution of total TN storage (kg N m⁻²) for the
326 circumpolar permafrost region for two depth intervals, 0-100 cm and 0-300 cm.

327 Table 6: Mean and total TN storage with 95% CI for the different depth increments for the northern circumpolar
328 permafrost region, excluding water bodies and permanent snow and ice.

Depth increment	Landscape mean TN storage (kg N/m²)		95% CI^a		Total TN in Pg	95% CI^a
0-30	271	0.5	±	0.1	8.1	± 1.5
0-50	250	0.7	±	0.1	12.3	± 2.5
0-100	208	1.2	±	0.3	21.1	± 4.7
100-200	175	1.0	±	0.2	17.1	± 2.8
200-300	169	0.9	±	0.2	16.8	± 3.7
0-300	169	3.1	±	0.8	55.0	± 15.1

329

330 ^a The 95% confidence interval refers to landscape mean TN storage and total TN storage



331 Table 7: Mean and total TN storage for (A) 0-100cm and (B) 0-300 soil depth separated for the different Tier classes
 332 within the northern circumpolar permafrost region, excluding water bodies and permanent snow and ice.

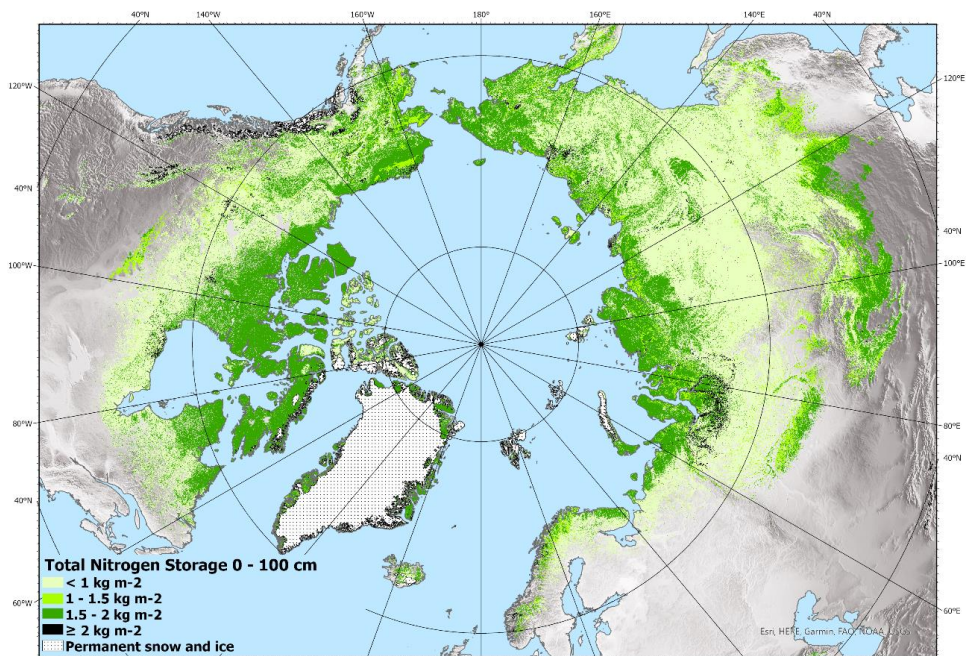
A	Tier class	LCC class	n^a:	Area (million km²)	Area %	Mean TN storage (kg N/m²)^b	SD_b	Total TN in Pg	Total TN storage %
	1.1	Deciduous forest broadleaf	2	0.85	4.8%	1.0	0.6	0.9	4.1
	1.2	Evergreen forest needleleaf	1	2.54	14.3%	0.8	0.8	1.9	9.2
	1.3	Deciduous forest needleleaf	19	5.20	29.1%	1.0	0.6	5.1	24.3
	2.1	Shrub tundra	32	3.97	22.3%	1.6	1.5	6.4	30.3
	2.2	Graminoid / forbtundra	72	2.85	15.9%	1.5	0.9	4.3	20.3
	3.1	Permafrost wetlands	46	0.25	1.4%	2.4	2.5	0.6	2.8
	3.2	Non-permafrost wetlands	4	0.76	4.3%	0.7	0.6	0.5	2.4
	5.1	Barren	26	0.85	4.8%	0.7	0.9	0.6	2.6
	7.1	Yedoma tundra	5	0.27	1.5%	1.6	0.6	0.4	2.0
	7.2	Yedoma forest	1	0.30	1.7%	1.4	0.0	0.4	2.0
B	Tier class	LCC class	n^a:	Area (million km²)	Area %	Mean TN storage (kg N/m²)^b	SD_b	Total TN in Pg	Total TN storage %
	1.1	Deciduous forest broadleaf	2	0.85	4.8%	2.8	1.7	2.4	4.3
	1.2	Evergreen forest needleleaf	1	2.54	14.3%	1.9	2.3	4.8	8.8
	1.3	Deciduous forest needleleaf	12	5.20	29.1%	2.4	1.3	12.6	23.0
	2.1	Shrub tundra	30	3.97	22.3%	3.9	3.4	15.5	28.2
	2.2	Graminoid / forbtundra	69	2.85	15.9%	3.4	2.2	9.6	17.5
	3.1	Permafrost wetlands	40	0.25	1.4%	7.0	7.8	1.8	3.2
	3.2	Non-permafrost wetlands	2	0.76	4.3%	6.4	6.6	4.9	8.9
	5.1	Barren	9	0.85	4.8%	0.8	1.1	0.7	1.2
	7.1	Yedoma tundra	3	0.27	1.5%	5.6	2.2	1.5	2.8
	7.2	Yedoma forest	1	0.30	1.7%	4.1	0.0	1.2	2.2

333

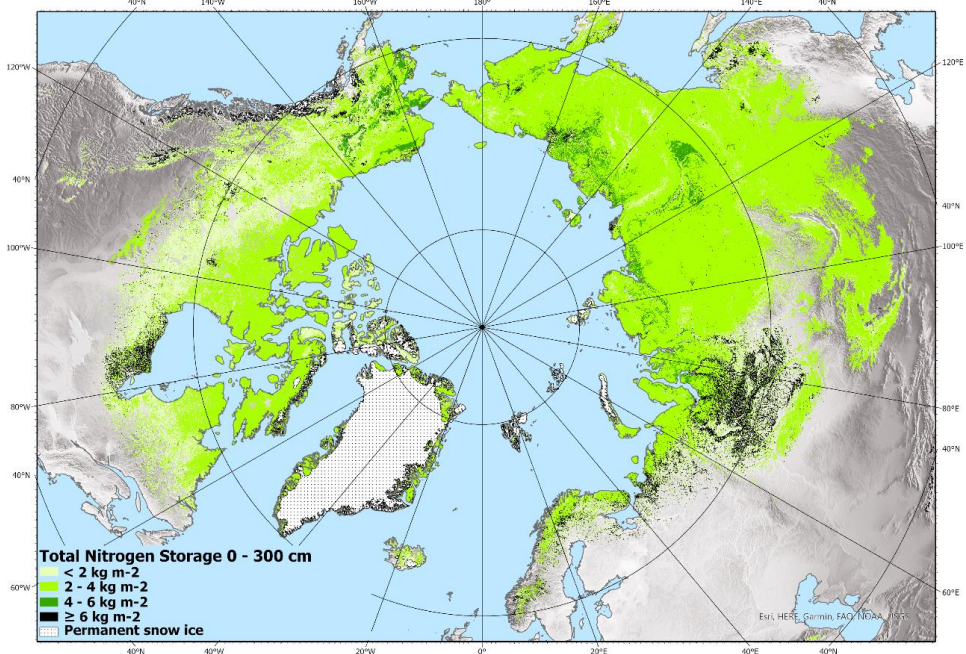
334 ^a The number of sampled pedons reaching a full depth of 100 cm or 300 cm, respectively.

335 ^b Mean TN storage and SD calculations includes pedons which are not reaching the full section depth.

336



337



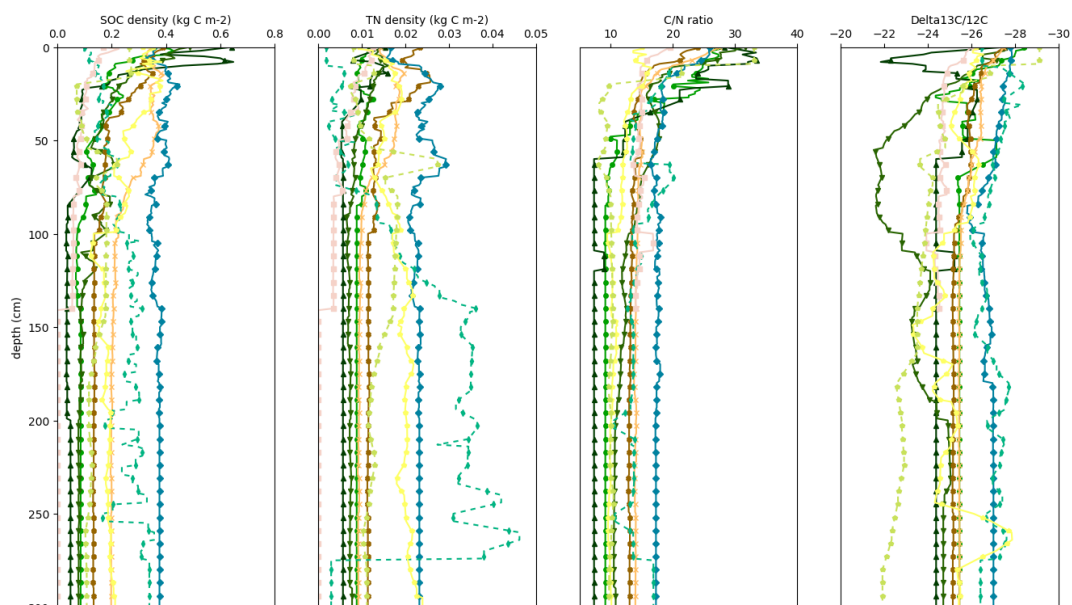
338

339 Figure 4. Estimated total Nitrogen storage (kg C m^{-2}) to a depth of 0-100 cm and 0-300 cm in northern circumpolar
340 permafrost region. North Pole Lambert azimuthal equal area projection (datum: WGS 84). Base map: Made with
341 Natural Earth.



342 3.3 Typical vertical soil stratigraphies to 300 cm depth

343 Figure 5 illustrates averaged vertical soil stratigraphies for SOC and TN density, C/N ratio with $\delta^{13}C$, dry bulk density,
344 volumetric fractions for water/ice, organic, mineral, air and texture (sand, silt+clay fraction) separated by land cover
345 class to 300 cm depth. The data shows clear differences occurring in the more variable top meter in comparison to the
346 rather stable second and third meter. These important trends are more evident, e.g. high variability in water fraction
347 between classes or high silt+clay fraction, in Yedoma tundra. We note that mineral soil texture is mainly determined
348 by the parent material origin, which has not been accounted for in the generation of these profiles.



349
350

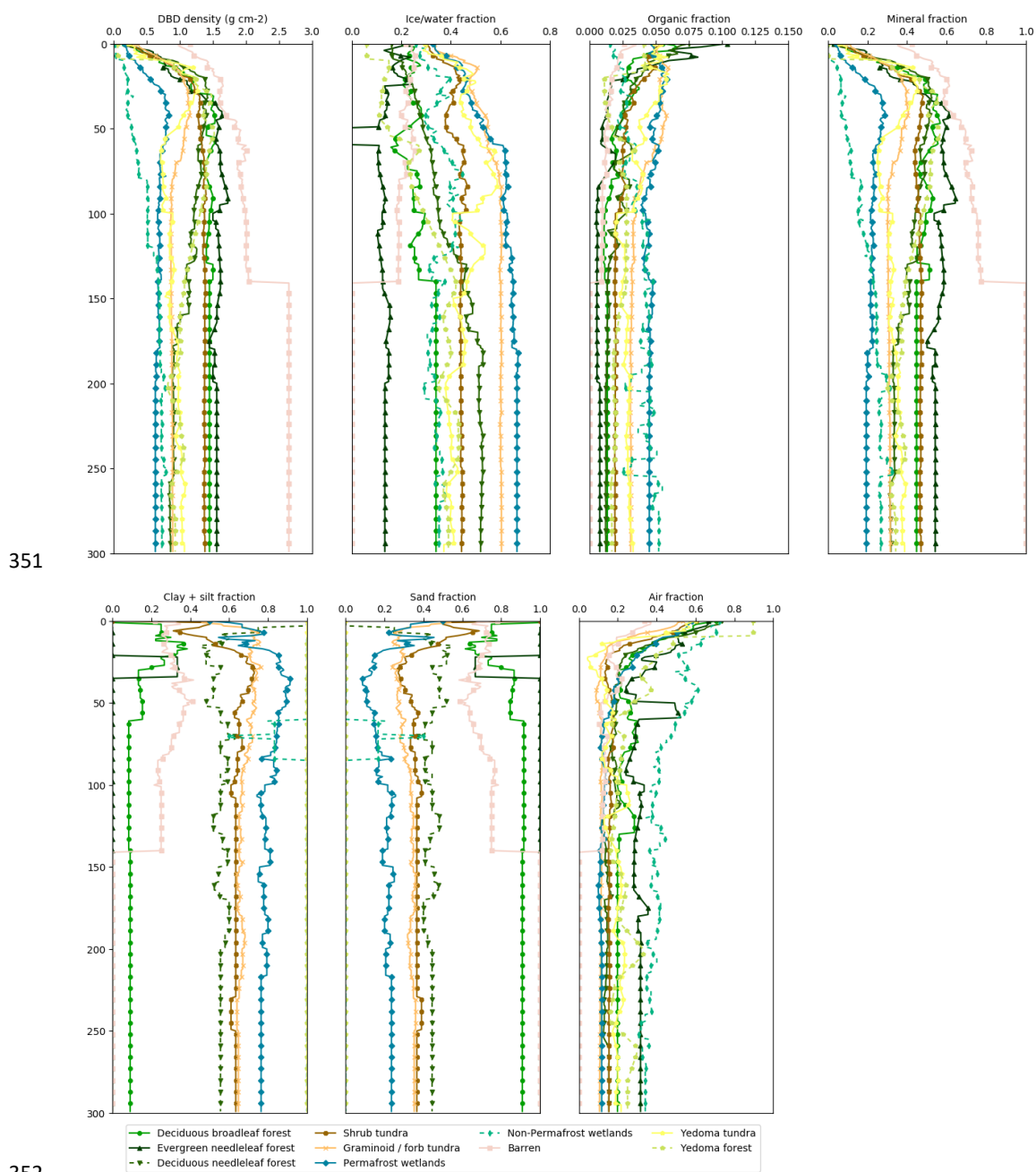


Figure 5. Typical vertical soil stratigraphies for all the land cover classes to 300 cm depth



354 4. Discussion

355 This new open access database was created to serve different scientific communities with high spatial resolution,
356 harmonized and georeferenced data on soil organic carbon and related key pedological parameters representative for
357 large areas across the northern permafrost region. Georeferenced and quality assessed soil profile data, with extensive
358 metadata will allow users to relate this field-data to various other ecosystem properties or processes. The goal of the
359 field studies to collect this dataset has mainly been to improve the knowledge base for studies of climate feedbacks
360 resulting from permafrost thaw. While there are multiple databases available containing data on soil carbon storage
361 (Hugelius et al., 2013, Michaelson et al., 2013, Mishra et al., 2021), there is still a lack of soil field data covering a
362 wider range of properties within the hard-accessible northern circumpolar permafrost region. This database provides
363 detailed high-resolution soil profile data on different key soil properties for both chemical (organic carbon, total
364 carbon, total nitrogen, d13C) and physical (dry and wet bulk density, soil texture, coarse fragments) parameters.

365 To test and exemplify usage of the soil profile database, we used our field-based metadata to classify soil profiles
366 according to a coherent land cover scheme and combined it with ESA's land cover product to provide a new estimate
367 of soil organic carbon storage in the northern circumpolar permafrost region. Our estimate for SOC is $380 \text{ Pg} \pm 58 \text{ Pg}$
368 to 100 cm soil depth and $813 \text{ Pg} \pm 136 \text{ Pg}$ to 300 cm soil depth for the permafrost region occupying an area of
369 $17.9 \times 10^6 \text{ km}^2$ (excluding area of Tibetan permafrost region, permanent snow and ice and water bodies). In
370 comparison, Hugelius et al., (2014) estimated SOC stocks in the northern circumpolar permafrost region (17.8×10^6
371 km^2 excluding exposed bedrock, glaciers and ice-sheets and water bodies) to be $472 \pm 27 \text{ Pg}$ and $1035 \pm 150 \text{ Pg}$ to
372 100 cm and 300 cm for soils, respectively. A recent publication by Mishra et al., (2021) based on >2700 soil profiles
373 with environmental variables in a geostatistical mapping framework, estimated a total SOC stock of 510 Pg (-78 to
374 $+79 \text{ Pg}$) and 1000 (-170 to $+186 \text{ Pg}$) to 100 cm and 300 cm, respectively. Despite different approaches in upscaling,
375 with Hugelius et al., (2014) using regional soil maps and Mishra et al., (2021) digital soil mapping, our landcover
376 based estimate is on the lower edge to previous studies. However, our estimates are still within each other's error
377 estimates. In comparison, this upscaling technique offers further benefits as this database can be easily extended with
378 additional sampling sites, higher-resolution land cover maps that will further increase the resolution on a circumpolar
379 scale. This data can also be used for upscaling in a particular area of interest.

380 Despite the importance of nitrogen for microbial decomposition and plant productivity processes, few large-scale
381 datasets are available on TN storage. Our TN estimate for the northern circumpolar permafrost region is $21 \text{ Pg} \pm 5 \text{ Pg}$
382 to 100 cm soil depth and $55 \text{ Pg} \pm 15 \text{ Pg}$ to 300 cm soil depth. This is in line with the only other circumpolar estimate
383 known to use by Harden et al. (2012) with a best estimate of 66 Pg ($\pm 35 \text{ Pg}$).

384 In addition, C/N ratio is a useful indicator of the organic matter decomposability which usually decreases with depth
385 with least decomposed material at the surface (organic layer) followed by carbon enriched (cryoturbated) pockets and
386 with smallest values and the most degraded material the mineral subsoil. Therefore, the C/N data together with the
387 d13C data locates the areas which are most likely to be more vulnerable to permafrost degradation which can be used
388 as a vulnerability map in combination with the botanical origin of the plant species using carbon isotopes.



389 A key element to this upscaling exercise is the accuracy of the land cover dataset. Despite the relatively high spatial
390 resolution of 300m, many Arctic landscape features cannot be represented at this scale. In addition, ESA's land cover
391 map has a good overall accuracy of 73%; however, this means that 27% of the land cover is possibly mismatched and
392 in need of improvement. Moreover, the accuracy for natural and semi-natural aquatic vegetation is unfortunately as
393 low as 19%. This corresponds to the class (wetland) with the largest SOC content in the permafrost region. According
394 to Hugelius et al. (2020), the areal extent of peatlands for the northern permafrost region ($3.7 \times 10^6 \text{ km}^2$) is almost four
395 times the ESA's land cover product estimated areal extent ($1.0 \times 10^6 \text{ km}^2$), used in this study. This would partly explain
396 our throughout lower estimate for SOC and TN on a circumpolar scale since the wetland classes have the largest SOC
397 and TN contents, particularly at greater depths (100-300 cm). If we correct the wetland area to $3.7 \times 10^6 \text{ km}^2$
398 ($2.0 \times 10^6 \text{ km}^2$ in permafrost-free peatlands and $1.7 \times 10^6 \text{ km}^2$ permafrost-affected peatlands) and deduct this in
399 proportion from the other classes, our updated SOC and TN stock to 300 cm soil depth increases to $954 \text{ Pg} \pm 162 \text{ Pg}$
400 and $66 \text{ Pg} \pm 22 \text{ Pg}$, respectively.

401 To our knowledge, this is the first product which presents different key soil properties and parameters on a circumpolar
402 scale even though they are the ones that are commonly used to parameterize earth system models. With this database
403 we aim to provide georeferenced point data that can easily be implemented and used for geospatial analysis at a
404 circumpolar scale. This will assist to quantify and model ongoing pedological and ecological processes relevant to
405 climate change. Furthermore, this may help identifying regions that are more vulnerable to permafrost degradation
406 and greenhouse gas release due to knowledge on texture, water/ice content or SOC storage.

407 5. Conclusion

408 This dataset represents a substantial contribution of high-quality soil pedon data across the northern permafrost region.
409 Despite a different methodology, our estimates of total SOC are similar but on the lower edge to other recent numbers.
410 The lower estimates from our dataset are probably due to underestimated areal extent of northern peatlands in the ESA
411 Global Land Cover dataset. In addition to SOC data, we contribute with novel TN estimates for the different land
412 cover classes and depth increments. Our TN estimate to 300 cm soil depth ($55 \text{ Pg} \pm 15 \text{ Pg}$) is in line with the only
413 other product available on that scale. We provide data for a wide range of environments and geographical regions
414 across the permafrost region including georeferencing and metadata. This serves as a base that can be easily combined
415 and extended with data from other sources, as several regions are underrepresented (Alaska, Canada, Tibet). This
416 dataset offers high scientific value as it also contains data on chemical and physical soil properties across the northern
417 circumpolar permafrost region. This additional data is of high importance and can be used to develop or parametrize
418 broad scale models and to help better understand different aspects of the permafrost-carbon climate feedback.

419 6. Data access

420 Two separated datasets (Detailed pedon data on soil carbon and nitrogen for the northern permafrost region,
421 <https://doi.org/10.17043/palmtag-2022-pedon-1>) (Palmtag et al., 2022a) and (A high spatial resolution soil carbon and



422 nitrogen dataset for the northern permafrost region, <https://doi.org/10.17043/palmtag-2022-spatial-1> with GeoTiffs
423 (Palmtag et al., 2022b) are freely available on the Bolin Centre data set repository (<https://bolin.su.se/data/>).

424

425 **Funding**

426 This study was funded through the European Space Agency CCI + Permafrost project (4000123681/18/I-NB), the
427 European Union Horizon 2020 research and innovation project Nunataryuk (773421), the Changing Arctic Ocean
428 (CAO) program project CACOON (NE/R012806/1) and the Swedish Research Council (2018-04516).

429

430 **Author contribution**

431 GH, PK, SW and JP designed the concept of the study. JO wrote the script in Python. JP wrote the initial draft of the
432 manuscript. All authors contributed to the writing and editing of the manuscript.

433 **Competing Interests**

434 The authors declare that they have no conflict of interest.

435 **Acknowledgements**

436 We thank the ESA CCI Land Cover project for providing the data, which was used for upscaling our product to
437 circumpolar scale.

438 **References**

- 439 Batjes, N.H.: Harmonized soil property values for broad-scale modelling (WISE30sec) with estimates of global soil
440 carbon stocks, *Geoderma*, Vol. 269, doi.org/10.1016/j.geoderma.2016.01.034, 2016.
- 441 Biskaborn, B. K., Smith, S. L., Noetzli, J., Matthes, H., Vieira, G., Streletskiy, D. A., Schoeneich, P., Romanovsky,
442 V. E., Lewkowitz, A. G., Abramov, A., Allard, M., Boike, J., Cable, W. L., Christiansen, H. H., Delaloye, R.,
443 Diekmann, B., Drozdov, D., Etzelmüller, B., Grosse, G., Guglielmin, M., Thomas Ingeman-Nielsen, T., Ketil Isaksen,
444 K., Ishikawa, M., Johansson, M., Johannsson, H., Joo, A., Kaverin, D., Kholodov, A., Konstantinov, P., Kröger, T.,
445 Lambiel, C., Lanckman, J.-P., Luo, D., Malkova, G., Meiklejohn, I., Moskalenko, N., Oliva, M., Phillips, M., Ramos,
446 M., Sannel, A. B. K., Sergeev, D., Seybold, C., Skryabin, P., Vasiliev, A., Wu, Q., Yoshikawa, K., Zheleznyak, M.



- 447 and Lantuit, H.: Permafrost is warming at a global scale, *Nature Communications*, 10(1), 264, 10.1038/s41467-018-
448 08240-4, 2019.
- 449 Czekirda, J., Westermann, S., Etzelmüller, B. and Johanneson, T.: Transient modelling of permafrost distribution in
450 Iceland. *Frontiers in Earth Science*, 7, 130, doi.org/10.3389/feart.2019.00130, 2019.
- 451 Defourny, P., Schouten, L., Bartalev, S.A., Bontemps, S., Caccetta, P., de Wit, A.J.W., Di Bella, C., Gerard, B., Giri,
452 C., Gong, V., Hazeu, G.W., Heinemann, A., Herold, M., Knoops, J., Jaffrain, G., Latifovic, R., Lin, H., Mayaux, P.,
453 Mâcher, C.A., Nonguierma, A., Stibig, H.J., Van Bogaert, E., Vancutsem, C., Bicheron, P., Leroy, M. and Arino, O.:
454 Accuracy assessment of a 300 m global land cover map: The GlobCover experience. Available online: [http://www.un-
455 spider.org/space-application/space-application-matrix/accuracy-assessment-300-m-global-land-cover-map-
456 globcover](http://www.un-spider.org/space-application/space-application-matrix/accuracy-assessment-300-m-global-land-cover-map-globcover) (accessed on 07 January 2022), 2008.
- 457 ESA Climate Change Initiative-Landcover visualization interface, Available from:
458 <http://maps.elie.ucl.ac.be/CCI/viewer/index.php> (accessed on 07 January 2022), 2017.
- 459 Farouki, O. T.: Thermal Properties of Soils, Cold regions research and engineering lab Hanover NH [online] Available
460 from: <https://apps.dtic.mil/docs/citations/ADA111734> (accessed on 07 January 2022), 1981.
- 461 Flato, G. M.: Earth system models: an overview, 2, 783–800, <https://doi.org/10.1002/wcc.148>, 2011.
- 462 Fritz, M., Vonk, J.E. and Lantuit, H.: Collapsing Arctic coastlines, *Nature Climate Change*, volume 7,
463 <https://doi.org/10.1038/nclimate3188>, 2017.
- 464 Fuchs, M., Kuhry, P., and Hugelius, G.: Low below-ground organic carbon storage in a subarctic Alpine permafrost
465 environment, *The Cryosphere*, 9, 427–438, <https://doi.org/10.5194/tc-9-427-2015>, 2015.
- 466 Global Soil Data Task: Global soil data products CD-ROM contents (IGBP-DIS), ORNL DAAC, 2014.
- 467 Gruber, S.: Derivation and analysis of a high-resolution estimate of global permafrost zonation, *The Cryosphere*, 6,
468 221–233, <https://doi.org/10.5194/tc-6-221-2012>, 2012.
- 469 Harden, J.W., Koven, C.D., Ping, C.-L., Hugelius, G., McGuire, A.D., Camill, P., Jorgenson, T., Kuhry, P.,
470 Michaelson, G.J., O'Donnell, J.A., Schuur, E.A.G., Tarnocai, C., Johnson, K. and Grosse, G.: Field information links
471 permafrost carbon to physical vulnerabilities of thawing. *Geophysical Research Letter*, 39, L15704,
472 doi:10.1029/2012GL051958, 2012.
- 473 Heiri, O., Lotter, A. F., and Lemcke, G.: Loss on ignition as a method for estimating organic carbon and carbonate
474 content in sediments: reproduction and comparability of results. *J. Paleolimnol.*, 25, 101–110,
475 <https://doi.org/10.1023/a:1008119611481>, 2001.
- 476 Hugelius G. and Kuhry, P.: Landscape partitioning and environmental gradient analyses of soil organic carbon in a
477 permafrost environment. *Global Biogeochem. Cycles*, 23, GB3006, doi:10.1029/2008GB003419, 2009.



- 478 Hugelius G., Kuhry, P., Tarnocai, C. and Virtanen, T.: Soil organic carbon pools in a periglacial landscape: a case
479 study from the central Canadian Arctic. *Permafrost Periglac. Process.*, 21: 16-29. <https://doi.org/10.1002/ppp.677>,
480 2010.
- 481 Hugelius, G., Virtanen, T., Kaverin, D., Pastukhov, A., Rivkin, F., Marchenko, S., Romanovsky, V. and Kuhry, P.:
482 High-resolution mapping of ecosystem carbon storage and potential effects of permafrost thaw in periglacial terrain,
483 European Russian Arctic, *J. Geophys. Res.*, 116, G03024, doi:10.1029/2010JG001606, 2011.
- 484 Hugelius, G. 2012.: Spatial upscaling using thematic maps: An analysis of uncertainties in permafrost soil carbon
485 estimates. *Global Biogeochem Cycles* GB2026. doi:10.1029/2011GB004154.
- 486 Hugelius, G., Bockheim, J. G., Camill, P., Elberling, B., Grosse, G., Harden, J. W., Johnson, K., Jorgenson, T., Koven,
487 C. D., Kuhry, P., Michaelson, G., Mishra, U., Palmtag, J., Ping, C.-L., O'Donnell, J., Schirrmeister, L., Schuur, E. A.
488 G., Sheng, Y., Smith, L. C., Strauss, J., and Yu, Z.: A new data set for estimating organic carbon storage to 3 m depth
489 in soils of the northern circumpolar permafrost region. *Earth Syst. Sci. Data*, 5, 393–402, [https://doi.org/10.5194/essd-](https://doi.org/10.5194/essd-5-393-2013)
490 5-393-2013, 2013.
- 491 Hugelius, G., Strauss, J., Zubrzycki, S., Harden, J. W., Schuur, E. A. G., Ping, C.-L., Schirrmeister, L., Grosse, G.,
492 Michaelson, G. J., Koven, C. D., O'Donnell, J. A., Elberling, B., Mishra, U., Camill, P., Yu, Z., Palmtag, J., and Kuhry,
493 P.: Estimated stocks of circumpolar permafrost carbon with quantified uncertainty ranges and identified data gaps.
494 *Biogeosciences* 11(23):6573– 6593, DOI: 10.5194/bg-11-6573-2014, 2014.
- 495 Hugelius, G., Loisel, J., Chadburn, S., Jackson, R.B., Jones, M., MacDonald, G., Marushchak, M., Olefeldt, D.,
496 Packalen, M., Siewert, M.B., Treat, C., Turetsky, M., Voigt, C. and Yu, Z.: Large stocks of peatland carbon and
497 nitrogen are vulnerable to permafrost thaw. *PNAS*, 117, 34, www.pnas.org/cgi/doi/10.1073/pnas.1916387117, 2020.
- 498 Köchy, M., Hiederer, R., and Freibauer, A.: Global distribution of soil organic carbon – Part 1: Masses and frequency
499 distributions of SOC stocks for the tropics, permafrost regions, wetlands, and the world, *SOIL*, 1, 351–365,
500 <https://doi.org/10.5194/soil-1-351-2015>, 2015.
- 501 Kracht, O and Gleixner, G.: Isotope analysis of pyrolysis products from Sphagnum peat and dissolved organic matter
502 from bog water. *Organic Geochemistry*, 31: 645–654, 2020.
- 503 Kuhry, P. and Vitt, D.H.: Fossil Carbon/Nitrogen Ratios as a Measure of Peat Decomposition. *Ecology*, 77: 271-275.
504 <https://doi.org/10.2307/2265676>, 1996.
- 505 Kuhry, P., Mazhitova, G.G., Forest, P.-A., Deneva, S.V., Virtanen, T. and Kultti, S.: Upscaling soil organic carbon
506 estimates for the Usa Basin (Northeast European Russia) using GIS-based land cover and soil classification schemes.
507 *Geografisk Tidsskrift-Danish Journal of Geography*, 102:1, 11-25, DOI: 10.1080/00167223.2002.10649462, 2002.
- 508 McKinney, W.: "pandas: a foundational Python library for data analysis and statistics." *Python for high performance*
509 *and scientific computing* 14.9, 1-9, 2011.



- 510 Michaelson, G.J., Ping, C.-L. and Clark, M.: Soil Pedon Carbon and Nitrogen Data for Alaska: An Analysis and
511 Update. *Open Journal of Soil Science*, 2013, 3, 132-142 <http://dx.doi.org/10.4236/ojss.2013.32015>, 2013.
- 512 Mishra, U., Hugelius, G., Shelef, E., Yang, Y., Strauss, J., Lupachev, A., Harden, J.W., Jastrow, J.D., Ping, C.-L.,
513 Riley, W.J., Schuur, E.A.G., Matamala, R., Siewert, M., Nave, L.E., Koven, C.D., Fuchs, M., Palmtag, J., Kuhry, P.,
514 Treat, C.C., Zubrzycki, S., Hoffman, F.M., Elberling, B., Camill, P., Veremeeva, A. and Orr, A.: Spatial heterogeneity
515 and environmental predictors of permafrost region soil organic carbon stocks. *Science Advances*, 7, 9, DOI:
516 10.1126/sciadv.aaz5236, 2021.
- 517 Nachtergaele, F., van Velthuisen, H., Verelst, L., Batjes, N.H., Dijkshoorn, K., van Engelen, V.W.P., Fischer, G.,
518 Jones, A. and Montanarella, L.: The harmonized world soil database, in Proceedings of the 19th World Congress of
519 Soil Science, Soil Solutions for a Changing World, Brisbane, Australia, 1-6 August 2010, pp. 34–37, 2010.
- 520 Obu, J., Westermann, S., Bartsch, A., Berdnikov, N., Christiansen, H.H., Dashtseren, A., Delaloye, R., Elberling, B.,
521 Eitzmuller, B., Kholodov, A., Khomutov, A., Kääb, A., Leibman, M.O., Lewkowicz, A.G., Panda, S.K.,
522 Romanovsky, V., Way, R.G., Westergaard-Nielsen, A., Wu, T., Yamkhin, J. and Zou, D.: Northern Hemisphere
523 permafrost map based on TTOP modelling for 2000–2016 at 1 km² scale, *Earth-Science Reviews* 193,
524 <https://doi.org/10.1016/j.earscirev.2019.04.023>, 2019.
- 525 Obu, J.: How much of the Earth's surface is underlain by permafrost? *Journal of Geophysical Research: Earth Surface*,
526 126, e2021JF006123. <https://doi.org/10.1029/2021JF006123>, 2021
- 527 Oleson, K. W., Lawrence, D. M., Bonan, G.B., Flanner, M.G., Kluzek, E., Lawrence, P.J., Levis, S., Swenson, S.C.,
528 Thornton, P.E., Dai, A., Decker, M., Dickinson, R., Feddema, J., Heald, C.L., Hoffman, F., Lamarque, J.-F.,
529 Mahowald, N., Niu, G.-Y., Qian, T., Randerson, J., Running, S., Sakaguchi, K., Slater, A., Stockli, R., Wang, A.,
530 Yang, Z.-L., Zeng, X., and Zeng, X.: Technical description of version 4.0 of the Community Land Model (CLM),
531 2010.
- 532 Palmtag, J., Hugelius, G., Lashchinskiy, N., Tarmstorf, M.P., Richter, A., Elberling, B. and Kuhry, P.: Storage,
533 landscape distribution and burial history of soil organic matter in contrasting areas of continuous permafrost, *Arct.*
534 *Antarct. Alp. Res.*, 47, 71–88, <https://doi.org/10.1657/AAAR0014-027>, 2015.
- 535 Palmtag, J., Ramage, J., Hugelius, G., Gentsch, N., Lashchinskiy, N., Richter, A. and Kuhry, P.: Controls on the
536 storage of organic carbon in permafrost soils in northern Siberia, *Eur. J. Soil Sci.*, 67, 478–491,
537 <https://doi.org/10.1111/ejss.12357>, 2016.
- 538 Palmtag, J. and Kuhry, P.: Grain size controls on cryoturbation and soil organic carbon density in permafrost-affected
539 soils. *Permafrost and Periglacial Process*, 29, <https://doi.org/10.1002/ppp.1975>, 2018.
- 540 Palmtag, J., Obu, J., Kuhry, P., Siewert, M., Weiss, N. and Hugelius, G.: Detailed pedon data on soil carbon and
541 nitrogen for the northern permafrost region. Dataset version 1. Bolin Centre Database.
542 <https://doi.org/10.17043/palmtag-2022-pedon-1>, 2022a.



- 543 Palmtag, J., Obu, J., Kuhry, P., Siewert, M., Weiss, N. and Hugelius, G.: A high spatial resolution soil carbon and
544 nitrogen dataset for the northern permafrost region. Dataset version 1. Bolin Centre Database.
545 <https://doi.org/10.17043/palmtag-2022-spatial-1>, 2022b.
- 546 Pascual, D., Kuhry, P. and Raudina, T.: Soil organic carbon storage in a mountain permafrost area of Central Asia
547 (High Altai, Russia). *Ambio*. <https://doi.org/10.1007/s13280-020-01433-6>, 2020.
- 548 Pribyl, D. W.: A critical review of the conventional SOC to SOM conversion factor, *Geoderma*, 156(3), 75–83,
549 [doi:10.1016/j.geoderma.2010.02.003](https://doi.org/10.1016/j.geoderma.2010.02.003), 2010.
- 550 Siewert, M.B., Hanisch, J., Weiss, N., Kuhry, P., Maximov, T.C. and Hugelius, G.: Comparing carbon storage of
551 Siberian tundra and taiga permafrost ecosystems at very high spatial resolution. *JGR - Biogeosciences*, Volume 120,
552 <https://doi.org/10.1002/2015JG002999>, 2015.
- 553 Siewert, M.B., Hugelius, G., Heim, B. and Faucherre, S.: Landscape controls and vertical variability of soil organic
554 carbon storage in permafrost-affected soils of the Lena River Delta. *CATENA*, Volume 147, Pages 725-741,
555 <https://doi.org/10.1016/j.catena.2016.07.048>, 2016.
- 556 Siewert, M. B.: High-resolution digital mapping of soil organic carbon in permafrost terrain using machine learning:
557 a case study in a sub-Arctic peatland environment, *Biogeosciences*, 15, 1663–1682, [https://doi.org/10.5194/bg-15-](https://doi.org/10.5194/bg-15-1663-2018)
558 1663-2018, 2018.
- 559 Siewert, M.B., Lantuit, H., Richter, A. and Hugelius, G.: Permafrost Causes Unique Fine-Scale Spatial Variability
560 Across Tundra Soils. *Global Biogeochemical Cycles*, 35, e2020GB006659. <https://doi.org/10.1029/2020GB006659>,
561 2021.
- 562 Soil survey staff, 2014. Keys to Soil Taxonomy. United States Department of
563 Agriculture & Natural Resources Conservation Service, Washington, DC, 12th ed. edition. United States
564 Department of Agriculture & Natural Resources Conservation Service, Washington, DC, 12th ed. edition.
- 565 Strauss, J., Schirrmeyer, L., Grosse, G., Fortier, D., Hugelius, G., Knoblauch, C., Romanovsky, V., Schädel, C.,
566 Schneider von Deimling, T., Schuur, T.A.G., Shmelev, D., Ulrich, M. and Veremeeva, A.: Deep Yedoma permafrost:
567 A synthesis of depositional characteristics and carbon vulnerability, *Earth-Science Reviews*, Volume 172,
568 doi.org/10.1016/j.earscirev.2017.07.007, 2017.
- 569 Thomson, S.K. Sampling. New York: John Wiley, 343 pp., 1992.
- 570 Turetsky, M.R., Abbott, B.W., Jones, M.C., Anthony, K.W., Olefeldt, D., Schuur, T.A.G., Koven, C., McGuire, A.D.,
571 Grosse, G., Kuhry, P., Hugelius, G., Lawrence, D.M., Gibson, C. and Sannel, A.B.K.: Permafrost collapse is
572 accelerating carbon release. *Nature*, 569, DOI 10.1038/d41586-019-01313-4, 2019.
- 573 Weiss, N., Blok, D., Elberling, B., Hugelius, G., Jörgensen, C.J., Siewert, M.B. and Kuhry, P.: Thermokarst dynamics
574 and soil organic matter characteristics controlling initial carbon release from permafrost soils in the Siberian Yedoma
575 region. *Sedimentary Geology*, 340, 38-48, <https://doi.org/10.1016/j.sedgeo.2015.12.004>, 2016.



- 576 Weiss, N., Faucherre, S., Lampiris, N. and Wojcik, R.: Elevation-based upscaling of organic carbon stocks in High-
577 Arctic permafrost terrain: a storage and distribution assessment for Spitsbergen, Svalbard. *Polar Research*, 36, 2017.
- 578 Westermann, S., Schuler, T. V., Gislås, K. and Etzelmüller, B.: Transient thermal modeling of permafrost conditions
579 in Southern Norway, *The Cryosphere*, 7, 719–739, <https://doi.org/10.5194/tc-7-719-2013>, 2013.
- 580 Westermann, S., Peter, M., Langer, M., Schwamborn, G., Schirrmeister, L., Etzelmüller, B., and Boike, J.: Transient
581 modeling of the ground thermal conditions using satellite data in the Lena River delta, Siberia, *The Cryosphere*, 11,
582 1441–1463, doi.org/10.5194/tc-11-1441-2017, 2017.
- 583 Wojcik, R., Palmtag, J., Hugelius, G., Weiss, N. and Kuhry, P.: Landcover and landform-based upscaling of soil
584 organic carbon stocks on the Brøgger Peninsula, Svalbard, *Arctic, Antarctic, and Alpine Research*, 51:1, 40-57, DOI:
585 10.1080/15230430.2019.1570784, 2019.